Resistance to mechanically small fatigue crack growth in ultrafine grained interstitial-free steel fabricated by accumulative roll-bonding

doi: 10.1016/j.ijfatigue.2018.09.002

Resistance to mechanically small fatigue crack growth in ultrafine grained interstitial-free steel fabricated by accumulative roll-bonding

X. Lin[a], M. Koyama[a]*, S. Gao[b], N. Tsuji[b], K. Tsuzaki[a] and H. Noguchi[a]

[a] Kyushu University, 744 Motooka, Nishi-ku, Fukuoka-shi, Fukuoka 819-0395, Japan

[b] Department of Materials Science and Engineering, Kyoto University, Yoshida-honmachi, Sakyo-ku, Kyoto 606-8501, Japan

*Corresponding author: Motomichi Koyama. e-mail: koyama@mech.kyushu-u.ac.jp

Abstract

Effects of ultrafine grain refinement on fatigue crack growth were investigated using an interstitial-free (IF) steel with a grain size of 590 nm produced by accumulative roll bonding. The fatigue properties and associated microstructures were characterized by fully reversed bending fatigue tests, replica method coupled with optical microscopy, and electron backscattering diffraction measurements near the fracture surfaces. Compared with a coarse-grained IF steel tested at the same stress amplitude, the fatigue strength of ultrafine-grained steel was higher, which was attributed to an increase in hardness. Compared with the coarse-grained steel at the same ratio of stress amplitude to hardness, the crack growth rates in the ultrafine grained steel were higher in the short-crack regime because of the smaller crack roughness and perhaps the difference in the strain gradient at the crack tip.

Keywords: crack closure; crack shape; small crack; accumulative roll bonding; ultrafine-grained steel

1. Introduction

In general, high tensile strength is required to realize safe design of parts of structures, simultaneously realizing a reduction in their weights. Strengthening of metallic materials can be achieved via solution hardening [1], work hardening [2], precipitation hardening [3], and grain refinement hardening [4][5]. In particular, the grain refinement has attracted attentions because of preservation of toughness and ductility in fine-grained materials [6]. In particular, the grain refinement below 1 μm in ferritic steels increases their yield strength greater than 1 GPa [7]. The grain size smaller than 1 μm is referred to as ultrafine grain (UFG). The severe plastic deformation (SPD) in which logarithmic equivalent strain ($\varepsilon_{eq.}$) larger than 4.0 is applied to materials has been utilized to produce bulky UFG metals. Such huge plastic strains have been achieved by the use of special SPD processes, such as equal-channel angular pressing [8][9], high-pressure torsion [10][11], and accumulative rolling bonding (ARB) [12][13][14]. In particular, the ARB process can introduce large strains into sheet materials and can realize homogeneous UFG microstructures in the bulky sheets [13][14].

From a practical viewpoint, not only high tensile strength, but also high fatigue strength is required, because the fatigue strength determines the capacity of load allowed in structures. In general, the fatigue limit has been recognized to be half of the tensile strength in smooth specimens [15]. Therefore, the fatigue limit and the fatigue strength normally increase with the increase in the tensile strength [15]. However, the dependence of the fatigue limit on the tensile strength is not necessarily linear and monotonic; for example, in martensitic steels, the fatigue limit decreases with the increase in the tensile strength, which is in contrast to a feature in low-strength steels [15, 16]. Hence, we have to focus on the fatigue limit and strength when the tensile strength increases markedly. In this context, effects of the ultrafine grain refinement on the fatigue limit and strength must be considered towards practical applications of UFG materials. More specifically, in steels which are the most practically important alloys, the fatigue limit and strength are dominated by behaviors of crack initiation and propagation [15, 16]. Therefore, to clarify the nature of the effect of grain refinement on fatigue properties, we must investigate the behaviors of fatigue crack initiation and propagation.

The ARB process has been successfully applied to enhance tensile properties in metallic materials. One of successful examples of the ARB process is that in interstitial-free (IF) steels; specifically, the ARB-processed IF steels with grain sizes smaller than 1 μm show the yield strength higher than 600 MPa. However, the fatigue crack resistance in the ARB-processed IF steels has never been investigated in terms of a fatigue performance. Therefore, the present study emphasizes fatigue crack initiation and growth in an ARB-processed IF steel with an UFG microstructure. The fatigue crack initiation is a

hardness-dependent phenomenon [15][17]. The crucial factors affecting the fatigue crack growth are hardness and crack closure [18]. As the hardness increment has been empirically understood to increase fatigue strength [15], we expect a positive effect of ultrafine-grained microstructures on the fatigue crack resistance in terms of crack closure phenomenon.

Mechanisms of the fatigue crack closure have been reported to be plasticity-induced crack closure (PICC) [19], roughness-induced crack closure (RICC) [20], transformation-induced crack closure [21], oxidation-induced crack closure [22], etc. In ARB-processed IF steels, degrees of PICC and RICC are expected to change with ultra-grain refinement. PICC results from the formation of compressive residual stresses in the plastic wake associated with evolution of plastic zones [23]. RICC is attributed to the deflection of crack paths of which degree is dependent on morphology of microstructures and grain sizes [23]. Hence, in this paper, we mainly discuss the effects of grain refinement on the crack roughness and the evolution of plastic zones in an ARB-processed IF steel having ultrafine grained microstructures.

2. Experimental procedures

2.1 Material: accumulative roll bonding process

We received an IF steel with a chemical composition of Fe-0.002C-0.01Si-0.1Mn-0.005P-0.005S-0.04Ti-0.03Al-0.0015N (mass%). The IF steel was heavily deformed by ARB in this study. The principle of ARB has been reported previously [12][13]. The initial sheets approximately 4 mm thick had a fully-recrystallized microstructure with a mean grain size of 50 μm. First, the initial sheets were subjected to cold rolling to achieve a thickness of 1 mm. Subsequently, two pieces of the cold-rolled sheets with dimensions 1 mm in thickness, 50 mm in width, and 300 mm in length were stacked to be 2 mm in thickness after being subjected to degreasing and wire-brushing the contact surfaces. The stacked sheets were roll-bonded in thickness at 773 K. The roll-bonded specimens were thereafter cooled in water and cut into two pieces. The same procedures described above were repeated for up to 6 cycles. The rolling ratio of the first pass was approximately 40% reduction, and from the second pass, it was approximately 50% reduction (von Mises equivalent strain: ε=0.8). Finally, the ARB processed sheets were annealed at a temperature of 773 K for 1.8 ks. The Vickers hardness of the UFG steel fabricated by the ARB and annealing processes was 160 HV. In addition, a coarse-grained (CG) specimen of the IF steel was prepared by annealing the as-received sheet at 973 K for 3.6 ks. The annealing process reduces the Vickers hardness from 88 HV to 72 HV. Hereafter, the ARB-processed and CG specimens of the IF steels were referred to as UFG and CG steels, respectively.

2.2 Microstructure characterization

Microstructural observations were conducted using electron backscatter diffraction (EBSD) measurements in a scanning electron microscope (SEM) operated at an accelerating voltage of 20kV. The EBSD orientation mapping was carried out with a beam step size of 70 nm on sections perpendicular to the transverse direction (TD) and normal direction (ND) of the sheet. Specimens for the EBSD measurements were prepared by mechanical polishing with colloidal silica with a particle size of 60 nm.

2.3 Tensile and fatigue tests

Tensile specimens with gauge dimensions of width 3 mm, thickness 1 mm, and length 25 mm were cut from the UFG and CG steel sheets by electric discharge machining (EDM) as shown in Fig. 1(a). The tensile tests were conducted with three pieces of the specimens at room temperature at an initial strain rate of 10^{-3} s^{-1}. The strains were measured by using a video extensometer.

Fatigue test specimens were also cut by EDM with the geometry shown in Fig. 1(b). Double drill holes of diameter 50 μm and depth 50 μm were introduced at the center of the specimens in order to control the crack initiation site. Fatigue tests were performed with a plane bending fatigue testing machine at room temperature with a stress ratio of −1 and at a frequency of 20 Hz. The fatigue cracks were observed using optical microscopy via plastic replica technique. After the fatigue tests, the fracture surface was observed using a SEM at an accelerating voltage of 15 kV. In addition, fatigue-fractured specimens were mechanically polished from the side of the specimens as shown in Fig. 1(c) and subsequent EBSD measurements were performed at a distance of 100 μm from the bottom of the drill holes, with a beam step size of 70 nm and an accelerating voltage of 20 kV.

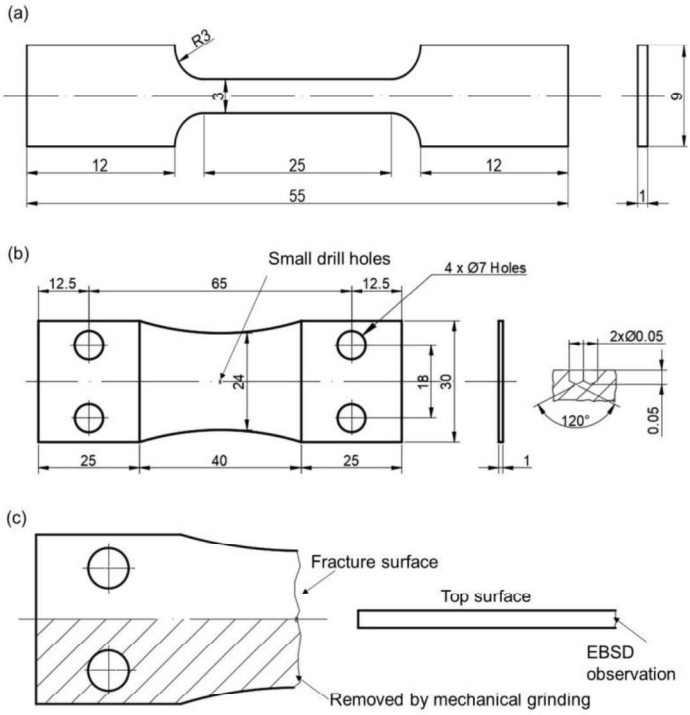

Fig. 1 Specimen geometries for (a) tensile and (b) bending fatigue tests, and (c) the region for EBSD observations.

The hatched region in (c) was removed via cutting and mechanical polishing.

3. Results

3.1 Microstructure before mechanical tests

Figure 2 shows microstructures obtained by EBSD orientation mapping of the CG and UFG IF steels before the mechanical tests. From Fig. 2(a), the average size of the equiaxed grains in the CG steel was measured to be 50 μm. The size and morphology of grains in the CG steel were homogeneous in the entire specimen. The grains near the surfaces of the UFG sheet were equiaxed, and their mean grain size was 0.71 μm. The grains at the center of the UFG sheet were elongated along the rolling direction as shown in Fig. 2 (c). The mean grain thickness of the UFGs was 0.59 μm. As reported in previous studies [13], the elongated UFGs were mostly surrounded by high-angle grain boundaries with misorientations larger than 15°, as is also shown in the EBSD maps (Fig.2 (c)).

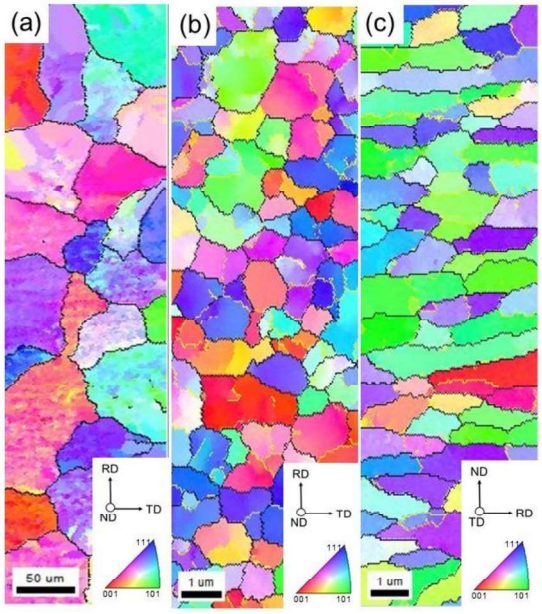

Fig. 2 (a) ND-IPF (inverse pole figure) map near the specimen surface of the CG steel. (b) ND map near the specimen surface, and (c) TD-IPF map at the center in the thickness direction of the UFG steel. The yellow and black lines indicate low- ($5<\theta\leq15$) and high-angle grain boundaries ($\theta>15$), respectively.

3.2 Tensile tests

Figure 3 shows engineering stress–engineering strain (SS) curves of the CG and UFG steels. The tensile strength reached to 660 MPa in the UFG steel, which is approximately 2.5 times higher than that of the CG steel. The CG steel showed smooth yielding, significant work hardening and uniform elongation. In contrast, the engineering flow stress of the UFG steel rapidly decreased immediately after the peak stress at a strain of 1.5%, corresponding to the occurrence of early plastic instability, which has been widely observed in UFG materials [14]. Subsequently, the engineering stress gradually decreased with the progress of macroscopic necking. The strength, elongation, and associated tensile behaviors have been reported in an IF steel ARB-processed with the same procedure as the present study [14]. The previous study reported that the extraordinary improvement of the strength by the present ARB process is attributed to mainly grain refinement and partly dislocation hardening [14]. The hardness increment in the UFG steel mentioned in the section 2.1 is also considered to stem from the same reason.

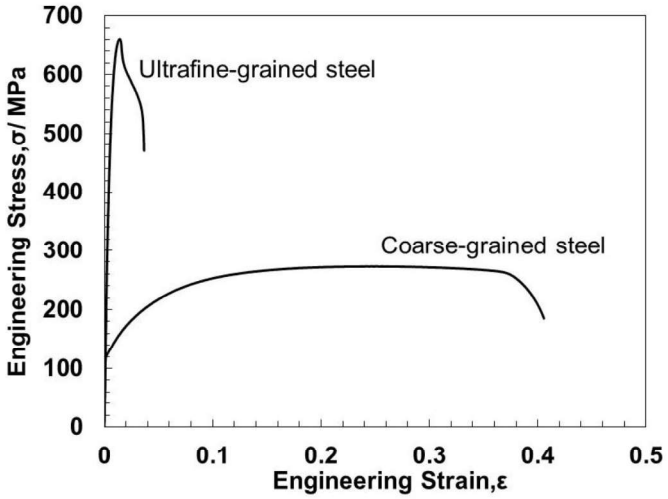

Fig. 3 Engineering stress versus engineering strain curves of the CG and UFG steels.

3.3 Stress amplitude versus number of cycles to failure diagrams

Figure 4(a) shows the number of cycles to failure plotted against stress amplitude in the CG and UFG steels. The fatigue limit is defined as the stress amplitude that does not result in failure at 2×10^7 cycles in this study. The fatigue limits for the CG and UFG steels were 140 MPa and 300 MPa, respectively. The differences in the fatigue limit and fatigue life are generally explained by hardness or tensile strength (Hardness or tensile strength has a better correlation with fatigue limit compared with yield strength, perhaps because the fatigue limit is controlled by both yielding and work hardening.) [15]. As long as the strengthening effect on fatigue is within a framework of general mechanisms, the fatigue limit and strength associated with mechanically small fatigue crack growth increase monotonically with tensile strength or hardness [15]. Therefore, to observe unconventional characters of fatigue behavior, we must compare the fatigue properties under the same relative mechanical driving force, i.e., stress amplitude normalized by tensile strength or hardness. Thus, the number of cycles to failure is plotted against stress amplitude normalized by hardness as shown in Fig. 4(b). The fatigue lives of the UFG steel as a function of normalized stress amplitude were almost identical to those of the CG steel. Moreover, the normalized fatigue limit of the UFG steel did not change significantly compared with that of the CG steel.

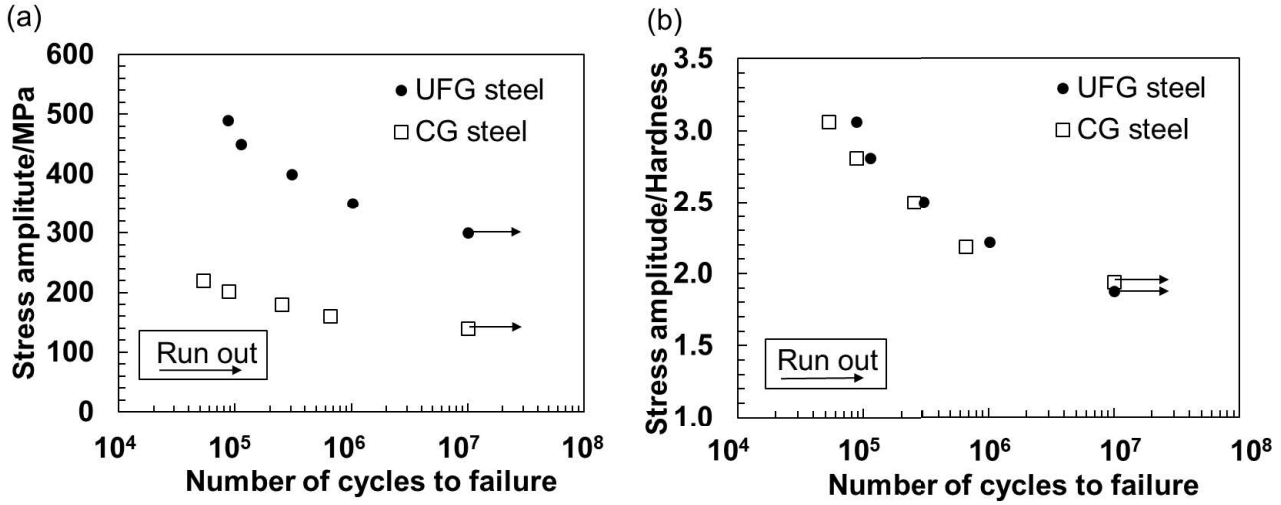

Fig. 4 (a) Stress amplitude versus fatigue lifetime curves of the CG and UFG steels. The stress amplitude was calculated from the maximum nominal stress. (b) Number of cycles to failure plotted against stress amplitude normalized by hardness.

3.4 Fatigue crack growth behavior

First note that no crack was initiated at the fatigue limits of the CG and UFG steels. Therefore, the fatigue limits of the IF steels under the present experimental condition are dominated by the crack initiation limits, although some previous experiments have shown fatigue limit associated with non-propagation of crack [24].

Figure 5(a) shows the crack growth curves for the CG and UFG steels at the stress amplitudes of 180 MPa and 400 MPa, respectively. From the crack length data, the fatigue crack growth rates (FCGR) were calculated as shown in Fig. 5(b). For a comparison at different stress amplitudes, the corresponding crack growth data at 490 MPa are presented in Figs. 5(c) and (d). The selected ratios between the stress amplitude and hardness in Figs. 5(a) and (c) were fixed at 2.5 and 3.06, respectively. The FCGR of the CG steel was lower than that of the UFG steel in the short-crack region. In contrast, in the long-crack region, the FCGR of the UFG steel was lower than that of the CG steel until fracture at both stress amplitude conditions. The lower FCGR of the UFG steel in the long-crack region results in longer fatigue life at the same normalized stress amplitude compared with that of the CG steel (Fig. 4). In fact, the lower FCGR of the UFG steel is attributed to crack coalescence in the CG steel, which will be discussed in section 4.3. Here, “short” and “long” indicate microstructurally short and long [25], respectively. Both microstructurally short and long cracks are mechanically small [26]. These definitions are mentioned here to avoid confusion, because we will later use the terms microstructurally short/long and mechanically small/large.

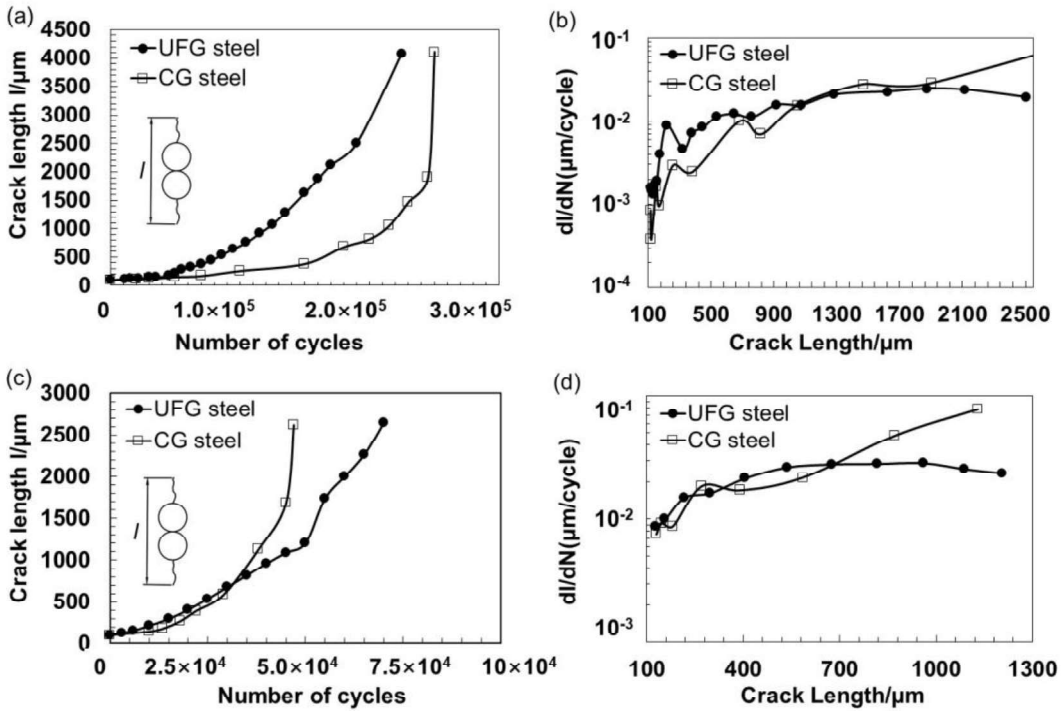

Fig. 5 FCGR curves of the two steels at the same ratio between stress amplitude and hardness. (a) Crack length versus number of cycles. (b) Crack growth rate versus crack length. Stress amplitudes of the CG and UFG steels are 180 MPa and 400 MPa (ratio between stress amplitude and hardness of 2.5), respectively. (c) Crack length versus number of cycles. (d) Crack growth rate versus crack length. Stress amplitudes of the CG and UFG steels are 220 MPa and 490 MPa (ratio between stress amplitude and hardness of 3.06), respectively.

Figures 6(a) and (b) show the replica images of short cracks (approximately 200 μm in total length) in the CG and UFG steels tested at 180 MPa and 400 MPa, respectively. The cracks in both the steels were initiated from the edges of the drill holes. In addition, slip bands distinctly formed around the drill hole, which were observed particularly in the CG steel as indicated by red arrows in Fig. 6(a).

When the crack propagated by more than 600 μm, a distinct difference in the plastic zone evolution near the fatigue crack was observed between the CG and UFG steels. In particular, in comparison with the UFG steel, the CG steel showed clearer contrast of slip lines, indicating a significantly heterogeneous plastic strain distribution, as shown in Fig. 7. Another important characteristic of the crack in the CG steel was the zigzag morphology, which affects crack closure behavior. The crack roughness of the CG steel remained when the crack propagated by more than 600 μm as shown in Fig. 7(a). Upon comparing the CG and UFG steels (Figs. 7(a) and (b)), a significant difference in crack roughness was observed. Even after propagation by more than 1 mm, significant crack roughness around the tip remained in the CG steel in comparison with the UFG steel, as

shown in Figs. 8(a) and (b). Moreover, slip bands were hardly observed in the replica optical images even in the long-crack region of the UFG steel. In addition, formation of sub-cracks was frequently observed in the CG steel, as indicated by red arrows in Fig. 8(a).

Figure 9 shows the results of EBSD measurements carried out 100 μm from the bottom of the drill hole in the fractured specimens used for obtaining Figs. 6 to 8. The grain reference orientation deviation (GROD) maps indicate strain distribution qualitatively. The EBSD data also show the significant difference in the deformation heterogeneity between the CG and UFG steels. Particularly, the CG steel exhibited significant GROD gradient from the fracture edge, as shown in Fig. 9(b). In contrast, the GROD gradient from the fracture edge was suppressed by the grain refinement, as shown in Fig. 9(d). In other words, the GRODs near the fracture edge in the CG steel are always higher than those in the region far from the fracture edge as predicted by simple mechanics. However, the UFG steel does not show a monotonic changing trend of GROD from the fracture edge, and shows even higher GRODs than those of the region far from the fracture edge.

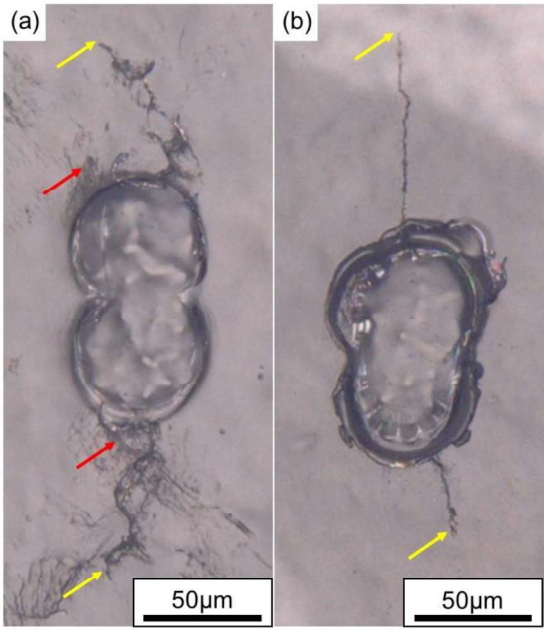

Fig. 6 Optical micrographs showing cracks of the (a) CG and (b) UFG steels tested at the stress amplitudes of 180 MPa and 400 MPa, respectively. The crack lengths of the CG and UFG steels are 229 μm and 219 μm, respectively. The yellow arrows indicate crack tips.

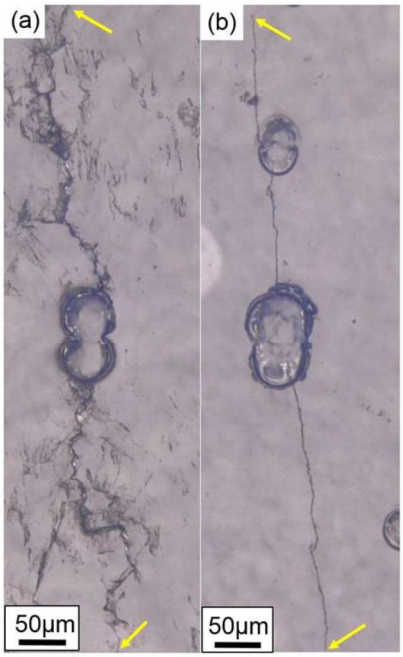

Fig. 7 Optical micrographs showing fatigue cracks of the (a) CG and (b) UFG steels tested at the stress amplitudes of 180 MPa and 400 MPa, respectively. The crack lengths of the CG and UFG steels are 679 μm and 631 μm, respectively. The yellow arrows indicate crack tips.

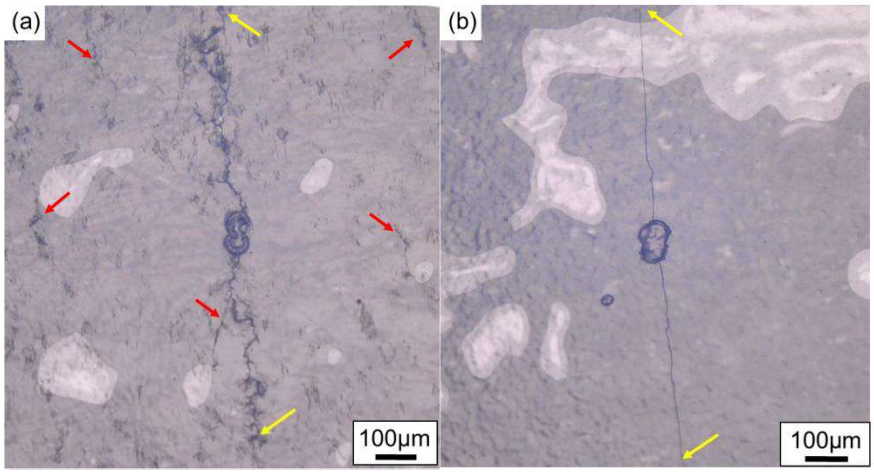

Fig. 8 Optical micrographs showing cracks of the (a) CG and (b) UFG steels tested at the stress amplitudes of 180 MPa and 400 MPa, respectively. The crack lengths of the CG and UFG steels are 1051 μm and 1075 μm, respectively. The yellow arrows indicate crack tips.

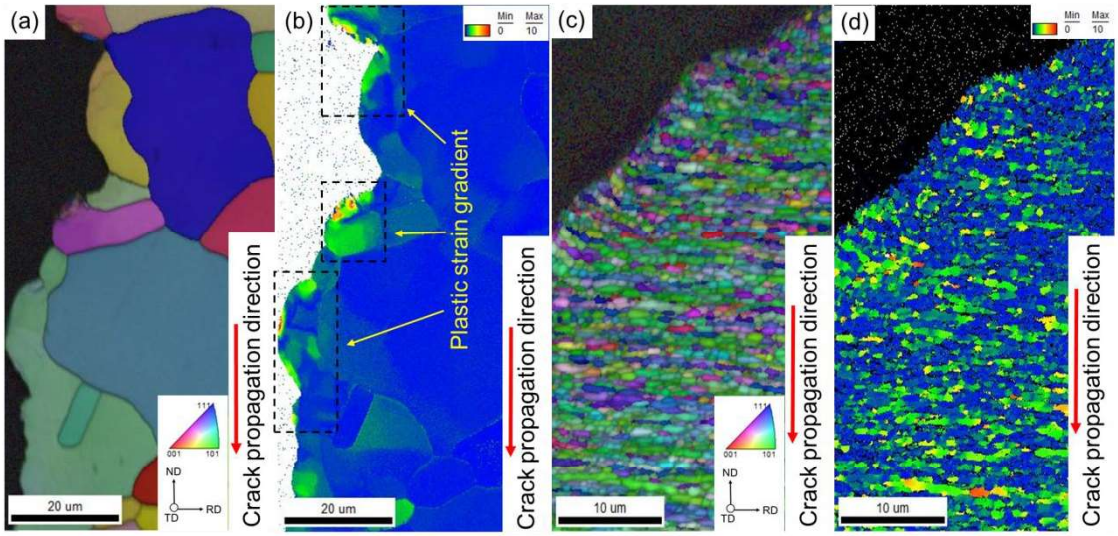

Fig. 9 EBSD results of a short-crack region 100 μm from the bottom of the drill holes in the CG and UFG steels tested at 180 MPa and 400 MPa, respectively. (a, c) TD-IPF maps with image quality contrast, and (b, d) GROD maps of the CG and UFG steels. The GROD, which qualitatively corresponds to plastic strain, is defined as difference between an orientation at an arbitrary point and an average orientation of each grain.

3.5 Fracture surface

Figures 10(a_1) and (b_1) show the overviews of fracture surfaces of the CG and UFG steels tested at the stress amplitudes of 180 MPa and 400 MPa, respectively. In the CG steel, intergranular and transgranular fracture modes were observed and several sub-cracks were formed in the long-crack region as indicated by yellow arrows in Fig 10(a_2). In addition, a river-like band was observed in the middle part of the fracture surface in the CG steel, as outlined by yellow dashed lines in Fig. 10(a_3). The river-like band implies the occurrence of crack coalescence. In particular, two cracks that initiated from the top and bottom surfaces where the tensile/compressive stress was the highest coalesced in the middle part where the tensile/compressive stress was approximately zero[1]. In the UFG steel, we could observe two characteristic points in terms of fractography. First, the fracture surface appeared smooth, or partly showed fine dimples as shown in Fig. 10(b_2). Therefore, we could not observe crystallographic and microstructural characteristics on the fractograph. Second, the overview image showed the occurrence of delamination events. The scale of the delamination event on the fracture surface was dependent on the location. For instance, distinct delamination was observed in the overview image as indicated by yellow arrows in Fig. 10(b_1), and a smaller scale

[1] As the cycles required for crack growth until 100 μm are skipped because of the presence of the initial crack (drill holes) on the top surface, the location of the river-like pattern is slightly shifted to the bottom side from the middle part.

delamination was observed as shown in Fig. 10(b_3).

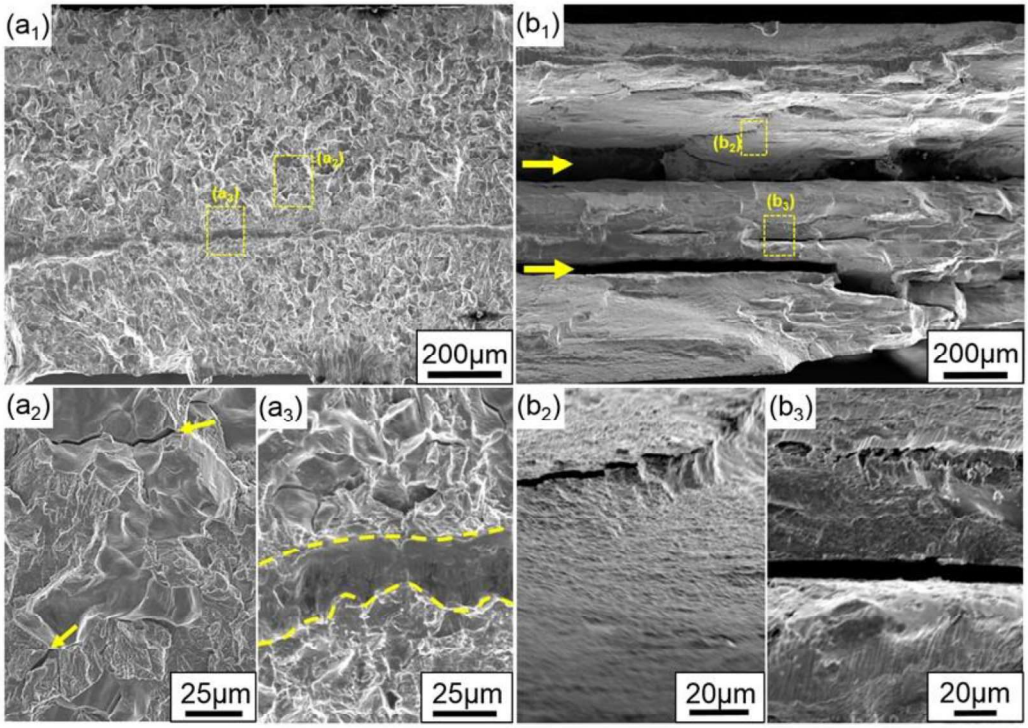

Fig. 10 SEM images of the overview fatigue fracture surfaces of the (a_1) CG and (b_1) UFG steels tested at the stress amplitudes of 180 MPa and 400 MPa, respectively. Magnified images showing (a_2) sub-cracks and (a_3) river-like band in the middle region outlined by yellow dashed lines in (a_1). Another set of magnified images showing (b_2) fine dimples and (b_3) delamination event in the regions outlined by yellow dashed lines in (b_1).

4. Discussion

4.1 Factors affecting fatigue limit and life associated with the grain refinement

First, we discuss the effect of grain refinement on the fatigue limit. As shown in Fig. 4(a), the fatigue limit was drastically improved with the grain refinement. As mentioned in the results section, the fatigue limits were determined by the crack initiation limits. The slip band formation and subsequent crack initiation shown in Fig. 6(a) indicate that the crack initiation in the steels was caused by a plasticity-driven mechanism. Therefore, the fatigue crack initiation limit of the UFG steel increased with the increases in the yield strength and hardness. Accordingly, the fatigue limit normalized by hardness was almost the same as that of the CG steel as demonstrated in Fig. 4(b).

Next, we note that the fatigue lives of the UFG steel were longer than those of the CG steel when compared at the same

stress amplitudes (Fig. 4(a)). At stress amplitudes above the fatigue limits, fatigue crack initiation occurred readily, indicating that the FCGR of the UFG steel was lower than that of the CG steel in the present plane bending tests. However, it has been reported that the grain refinement in an IF steel accelerates fatigue crack growth in compact tension (CT) tests [27]. A major difference between the CT tests and the present experiment is the crack length. When the crack length is mechanically large and small-scale yielding condition is satisfied, the FCGR does not have a direct correlation with the hardness or tensile strength [18]. Therefore, the FCGR in the CT tests is mainly dependent on the crack closure behavior. Grain refinement has been known to deteriorate the effects of crack closure such as RICC, thus accelerating the growth of the mechanically large crack [27]. In contrast, mechanically small fatigue crack growth, as in the case of the present study, strongly depends on the hardness [28][29]. Correspondingly, as indicated in Fig. 4(b), the fatigue limit and stress amplitudes corresponding to respective fatigue lives of the IF steel showed almost the same degree of improvements as the increment of hardness by the grain refinement. This fact indicates that the strengthening effect by grain refinement effectively contributes to the improvement of resistance to mechanically small crack growth. Hence, we conclude that the grain refinement negatively affects FCGR in a mechanically large crack, but positively affects FCGR in a mechanically small crack.

Furthermore, the FCGR of the UFG steel showed a slight difference from that of the CG steel at the same ratio of stress amplitude to hardness as shown in Figs. 5(a-d), although the fatigue lives were almost identical. Particularly, the FCGR of the short-crack region of the UFG steel was slightly higher, but the FCGR of the long-crack region was lower than that of the CG steel. In order to understand the specific crack growth behaviors, we must discuss the effects of crack roughness and plastic zone evolution on the crack closure and crack coalescence behavior.

4.2 Crack closure in the short fatigue crack growth region

In this section, we discuss why the FCGR of the UFG steel was higher than that of CG steel at the same stress amplitude normalized by hardness. In terms of crack closure, we consider the effects of crack roughness and plastic zone evolution, based on the replica images. In a previous paper on CT tests [27], grain refinement in an IF steel was reported to reduce the degree of crack roughness, which is consistent with the present work as demonstrated in Figs. 7 and 8. As the crack roughness is attributed to intergranular crack growth or crack growth along a slip plane [30], the roughness size approximately corresponds to the grain size. Therefore, the effect of grain refinement on crack roughness deteriorates the contribution of RICC. Another

factor causing crack roughness is small crack coalescence. As shown in Fig. 8, a considerable number of sub-cracks were observed in the CG steel, whereas the sub-crack formation was suppressed in the UFG steel. As the small crack coalescence results in tortuous crack morphology, the suppression of sub-crack formation by the grain refinement also reduces the effect of RICC on crack growth.

Furthermore, there is significant plastic strain heterogeneity in the CG steel in comparison with the UFG steel, which was revealed by the slip line observation in replicas (Fig. 7(a)). The GROD maps in Fig. 9 also support the presence of strain heterogeneity, particularly, the heterogeneity arising from the strain gradient from the crack surface. More specifically, the GROD values in the CG steel showed the monotonic decrease from the crack surface, and the GRODs in the region 10 μm far from the crack surface was almost zero. In contrast, the GRODs in the UFG steel did not show a monotonic decrease, and showed GRODs higher than 5˚ even in the region 10 μm far from the crack surface. Since GROD qualitatively corresponds to plastic strain, these results indicate that the grain refinement reduced a slope of the plastic strain gradient from the crack surface. Since plastic strain arises from dislocation motion, distribution of sources of dislocation emission and multiplication would be key to understand the reduction in a slope of the plastic strain gradient. It has been reported that, in the UFG steel, dislocations are emitted not only from the crack tip but also from the grain boundaries, resulting in higher mobile dislocation density compared with the CG steel [31]. To be more specific, according to a previous study on an interaction between a crack and dislocation motion in an ARB-processed UFG steel [32], dislocations emitted from a crack tip are impinged at grain boundaries, subsequently dislocations are re-emitted from the grain boundaries, namely, mobile dislocation density becomes high in both of the regions near the crack tip and beyond the grain boundaries. Since the dislocations impinged at grain boundaries cause shielding stress to the crack tip, further loading would cause plastic deformation preferentially beyond the grain boundaries. This consideration explains the suppression of strain gradient by the grain refinement observed in this study. The difference in plastic strain gradient can alter the PICC behavior. In particular, plastic strain gradient assists reverse yielding, recovering stress concentration at the crack tip and accelerating fatigue crack growth [33][34]. However, the forward and reverse yielding behaviors that depend on the strain gradient enhance the subsequent PICC effect in the following cycle because of more significant evolution of the plastic zone. As the former and latter effects are negative and positive for FCGR, respectively, concluding the significance of the plastic strain gradient on PICC requires further mechanical study in the future. In this study, we propose that the suppression of strain gradient by grain refinement can reduce the effect of PICC, which accelerates fatigue crack growth.

4.3 Effects of crack coalescence in the long-crack growth region: fractographic viewpoint

Here, we note the fact that total fatigue life of the UFG steel was almost identical or slightly longer than that of the CG steel at the same stress amplitude normalized by hardness (Fig. 4(b)), even though the FCGR of the UFG steel at the short-crack regime was higher (Fig. 5). The key to understand the fatigue behavior can be found in the long-crack growth. It is evident that numerous sub-cracks were formed on the top surface of the CG steel as shown in Fig. 8a, implying that the back surface also showed numerous sub-cracks. Assuming that the sub-cracks were formed readily on the back surface, the main crack that initiated from the drill hole on the top surface coalesced with one of the sub-cracks on the back surface, which formed a through crack, as schematically shown in Fig. 11(a). The river-like pattern appearing in the near-middle region of the fracture surface of the CG steel (Fig. 10a_3) demonstrates the coalescence of the long cracks formed from the top and back surfaces. In this context, the UFG steel does not suffer from the effect of coalescence of long cracks, because significant sub-crack formation was not observed in the UFG steel as shown in Fig. 8b. Therefore, the formation of through crack markedly accelerates the fatigue crack growth only in the CG steel [Figs. 5(b) and (d)].

Furthermore, we note the occurrence of delamination event of the fatigue crack growth in the UFG steel, shown in Figs. 10b_1 and b_3. The delamination events in the UFG steel are perhaps due to the shear stress associated with bending deformation during the fatigue test. In particular, the cyclic shear stress may cause the fatigue cracking along the bonding plane formed via the ARB process, although monotonic tension does not cause the delamination event. The delamination event results from crack deflection or crack branching, which therefore acts as a factor decelerating the fatigue crack growth. The combined effect of long crack coalescence in the CG steel and delamination event in the UFG steel resulted in the higher FCGR in the CG steel than that in the UFG steel.

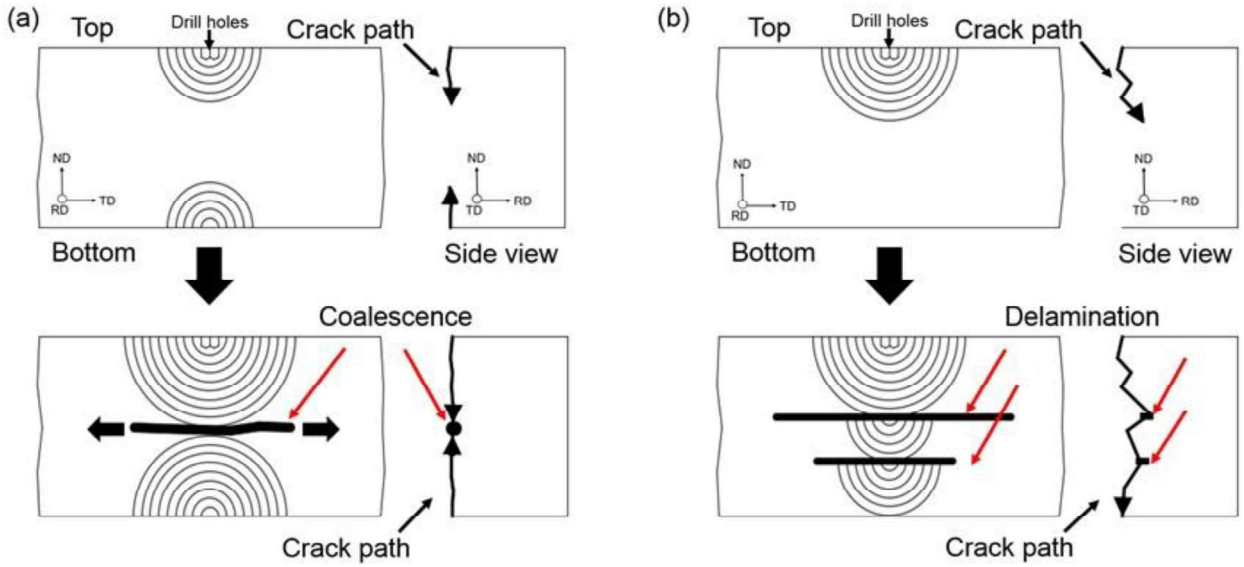

Fig. 11 Schematic illustrations of the fatigue crack propagation mechanisms of the (a) CG and (b) UFG steels.

5. Conclusions

The FCGRs of CG and UFG IF steels were examined in this study. The following conclusions could be drawn.

(1) The fatigue strength of the UFG steel was higher than that of the CG steel. In particular, the fatigue limits correspond to the fatigue crack initiation limits for the respective steels. Hence, the fatigue limit was enhanced by grain refinement via the improvement of plastic deformation resistance at a stress concentration source; in other words, the improvement is simply attributed to an increase in hardness.

(2) Although the increment of hardness by the grain refinement does not improve the fatigue crack growth resistance in a mechanically long crack according to the previous reports, the present work clarified that the resistance to the mechanically short crack growth is enhanced by the grain refinement strengthening.

(3) At stress amplitudes normalized by hardness, the crack growth rates of the CG steel were lower than those of the UFG steel in the short-crack regime. The deceleration of the crack growth in the CG steel is attributed to RICC. In addition, we suggest that the grain refinement might affect PICC behavior in terms of a change in the plastic strain gradient at the crack tip.

(4) In contrast, at a long crack, the UFG steel showed lower crack growth rates compared with those of the CG steel. Consequently, the fatigue lives of the UFG steel were longer than those of the CG steel even when plotted against

normalized stress amplitude. We propose that the origin of the high FCGRs in the long-crack regime in the CG steel is associated with the long crack coalescence, which resulted from the low resistance to crack initiation. Additionally, in the UFG steel, delamination formation can decelerate crack growth, which results in lower FCGR in the long-crack regime of the UFG steel than that in the CG steel.

Acknowledgments

This work was financially supported by JSPS KAKENHI (JP16H06365) and Elements Strategy Initiative for Structural Materials (ESISM) of Ministry of Education, Culture, Sports, Science and Technology (MEXT), Japan.

References

[1] Sato A, Meshii M. Solid solution softening and solid solution hardening. Acta Metall 1973;21:753–68. doi:10.1016/0001-6160(73)90040-0.

[2] Chen XH, Lu L. Work hardening of ultrafine-grained copper with nanoscale twins. Scr Mater 2007;57:133–6. doi:10.1016/j.scriptamat.2007.03.029.

[3] Gladman T. Precipitation hardening in metals. Mater Sci Technol 1999;15:30–6. doi:10.1179/026708399773002782.

[4] Estrin Y, Vinogradov A. Extreme grain refinement by severe plastic deformation: A wealth of challenging science. Acta Mater 2013;61:782–817. doi:10.1016/j.actamat.2012.10.038.

[5] Kawasaki M, Langdon TG. Principles of superplasticity in ultrafine-grained materials. J Mater Sci 2007;42:1782–96. doi:10.1007/s10853-006-0954-2.

[6] Terada D, Inoue S, Tsuji N. Microstructure and mechanical properties of commercial purity titanium severely deformed by ARB process. J Mater Sci 2007;42:1673–81. doi:10.1007/s10853-006-0909-7.

[7] Calcagnotto M, Adachi Y, Ponge D, Raabe D. Deformation and fracture mechanisms in fine- and ultrafine-grained ferrite/martensite dual-phase steels and the effect of aging. Acta Mater 2011;59:658–70. doi:10.1016/j.actamat.2010.10.002.

[8] Cornwall LR, Hartwig KT, Goforth RE, Semiatin SL. The equal channel angular extrusion process for materials processing. Mater Charact 1996;37:295–300. doi:10.1016/S1044-5803(97)80018-6.

[9] Iwahashi Y, Wang J, Horita Z, Nemoto M, Langdon TG. Principle of equal-channel angular pressing for the processing of ultra-fine grained materials. Scr Mater 1996;35:143–6. doi:10.1016/1359-6462(96)00107-8.

[10] Edalati K, Horita Z. A review on high-pressure torsion (HPT) from 1935 to 1988. Mater Sci Eng A 2016;652:325–52. doi:10.1016/j.msea.2015.11.074.

[11] Zhilyaev AP, Langdon TG. Using high-pressure torsion for metal processing: Fundamentals and applications. Prog Mater Sci 2008;53:893–979. doi:10.1016/j.pmatsci.2008.03.002.

[12] Saito Y, Utsunomiya H, Tsuji N, Sakai T. Novel ultra-high straining process for bulk materials—development of the accumulative roll-bonding (ARB) process. Acta Mater 1999;47:579–83. doi:10.1016/S1359-6454(98)00365-6.

[13] Tsuji N, Ueji R, Minamino Y. Nanoscale crystallographic analysis of ultrafine grained IF steel fabricated by ARB process. Scr Mater 2002;47:69–76. doi:10.1016/S1359-6462(02)00088-X.

[14] Tsuji N, Ito Y, Saito Y, Minamino Y. Strength and ductility of ultrafine grained aluminum and iron produced by ARB and annealing. Scr Mater 2002;47:893–9. doi:10.1016/S1359-6462(02)00282-8.

[15] Murakami Y. Metal fatigue: Effect of small defects and nonmetallic inclusions. Oxford: Elsevier; 2002.

[16] Hamano Y, Koyama M, Hamada S, Noguchi H. Notch sensitivity of the fatigue limit in high-strength steel. ISIJ Int 2016;56:1480–6. doi:10.2355/isijinternational.ISIJINT-2015-744.

[17] Miyazaki T, Noguchi H, Ogi K. Quantitative evaluation of fatigue limit of a metal with an arbitrary crack under a stress controlled condition (Stress Ratio = −1). Int J Fracture 2004;129:21-38. doi:10.1023/B:FRAC.0000038886.80094.59.

[18] Fukumura N, Suzuki T, Hamada S, Tsuzaki K, Noguchi H. Mechanical examination of crack length dependency and material dependency on threshold stress intensity factor range with Dugdale model. Eng Fract Mech 2015;135:168–86. doi:10.1016/j.engfracmech.2015.01.003.

[19] Vasudeven AK, Sadananda K, Louat N. A review of crack closure, fatigue crack threshold and related phenomena. Mater Sci Eng A 1994;188:1–22. doi:10.1016/0921-5093(94)90351-4.

[20] Suresh S, Ritchie RO. A Geometric model for fatigue crack closure induced by fracture surface roughness. Metall Trans A 1982;13:1627–31. doi:10.1007/BF02644803.

[21] Pineau AG, Pelloux RM. Influence of strain-induced martensitic transformations on fatigue crack growth rates in stainless steels. Metall Trans 1974;5:1103–12. doi:10.1007/BF02644322.

[22] Suresh S, Zamiski GF, Ritchie DRO. Oxide-Induced Crack Closure: An Explanation for Near-Threshold Corrosion Fatigue

Crack Growth Behavior. Metall Trans A 1981;12:1435–43. doi:10.1007/BF02643688.

[23] Parry MR, Syngellakis S, Sinclair I. Numerical modelling of combined roughness and plasticity induced crack closure effects in fatigue. Mater Sci Eng A 2000;291:224–34. doi:10.1016/S0921-5093(00)00971-0.

[24] Li B, Koyama M, Sakurada E, Yoshimura N, Ushioda K, Noguchi H. Temperature dependence of transgranular fatigue crack resistance in interstitial-free steel and Fe-C steels with supersaturated carbon: Effects of dynamic strain aging and dynamic precipitation. Int J Fatigue 2018;110:1–9. doi:10.1016/j.ijfatigue.2018.01.003.

[25] Ritchie RO, Lankford J. Small fatigue cracks: A statement of the problem and potential solutions. Mater Sci Eng 1986;84:11–6. doi:10.1016/0025-5416(86)90217-X.

[26] Nisitani H, Goto M, Kawagoishi N. A small-crack growth law and its related phenomena. Eng Fract Mech 1992;41:499–513. doi:10.1016/0013-7944(92)90297-R.

[27] Niendorf T, Rubitschek F, Maier HJ, Canadinc D, Karaman I. On the fatigue crack growth-microstructure relationship in ultrafine-grained interstitial-free steel. J Mater Sci 2010;45:4813–21. doi:10.1007/s10853-010-4511-7.

[28] Fukumura N, Suzuki T, Hamada S, Tsuzaki K, Noguchi H. Mechanical examination of crack length dependency and material dependency on threshold stress intensity factor range with Dugdale model. Eng Fract Mech 2015;135:168–86. doi:10.1016/j.engfracmech.2015.01.003.

[29] Koyama M, Yamamura Y, Sawaguchi T, Tsuzaki K, Noguchi H. Microstructural hardness heterogeneity triggers fatigue crack non-propagation in as-hot-rolled Fe-30Mn-3Si-3Al twinning-induced plasticity steel. Int J Fatigue 2018;108:18–24. doi:10.1016/j.ijfatigue.2017.11.009.

[30] Weinberger CR, Boyce BL, Battaile CC. Slip planes in bcc transition metals. Int Mater Rev 2013;58:296–314. doi:10.1179/1743280412Y.0000000015.

[31] Shimokawa T, Tanaka M, Kinoshita K, Higashida K. Roles of grain boundaries in improving fracture toughness of ultrafine-grained metals. Phys Rev B 2011;83:1–13. doi:10.1103/PhysRevB.83.214113.

[32] Tanaka M, Higashida K, Shimokawa T, Morikawa T. Brittle-ductile transition in low carbon steel deformed by the accumulative roll bonding process. Mater Trans 2009;56:56-63. doi:10.2320/matertrans.MD200817.

[33] Budiansky B, Hutchinson J.W, Analysis of closure in fatigue crack growth. J Appl Mech 1978;45:267-76. doi:10.1115/1.3424286.

[34] Rice J.R, Mechanics of crack tip deformation and extension by fatigue. Fatigue Crack Propag 1967;ASTM STP 4:247–309.

doi:10.1520/STP47234S.

Figure
Click here to download high resolution image

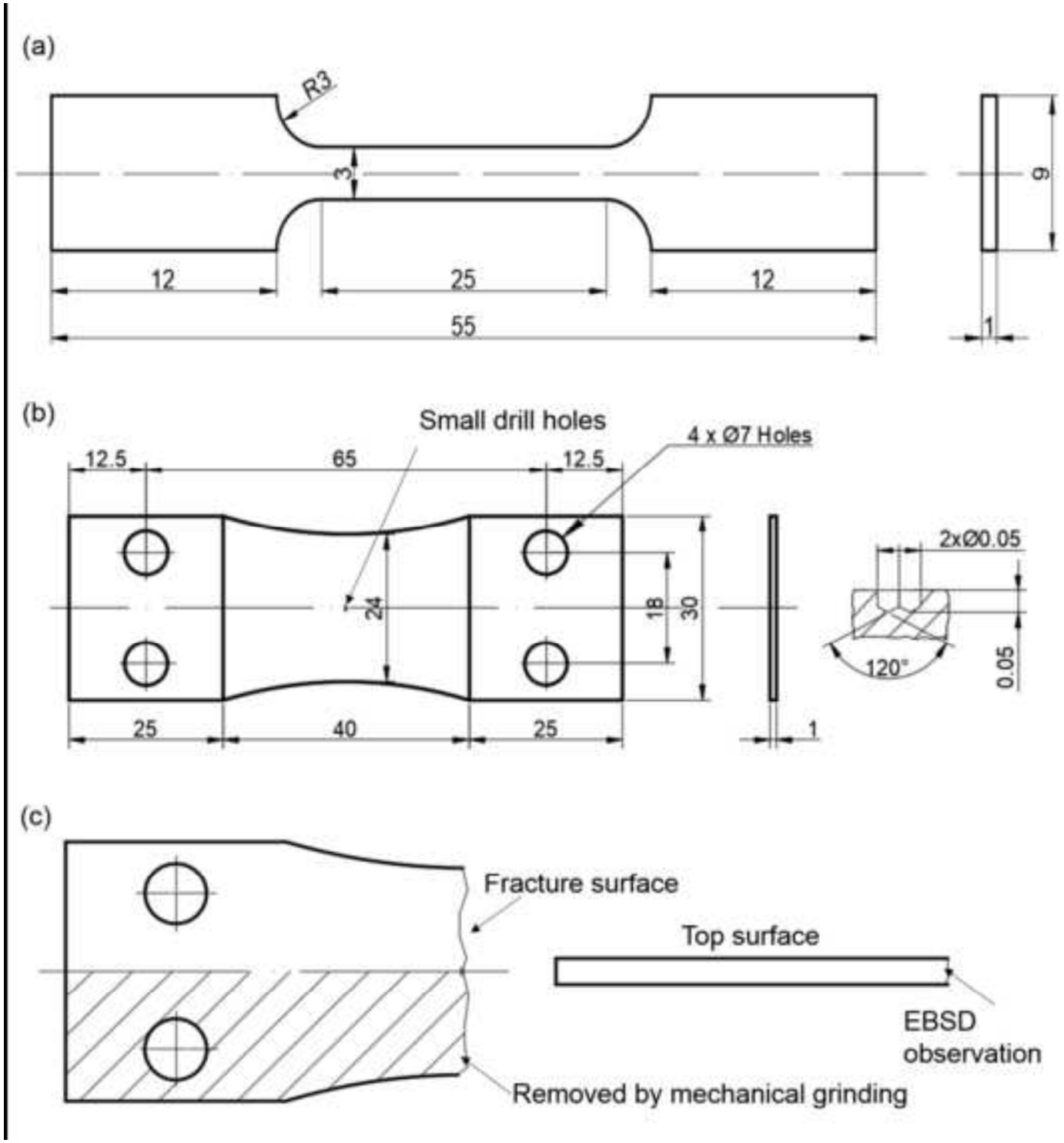

Figure
Click here to download high resolution image

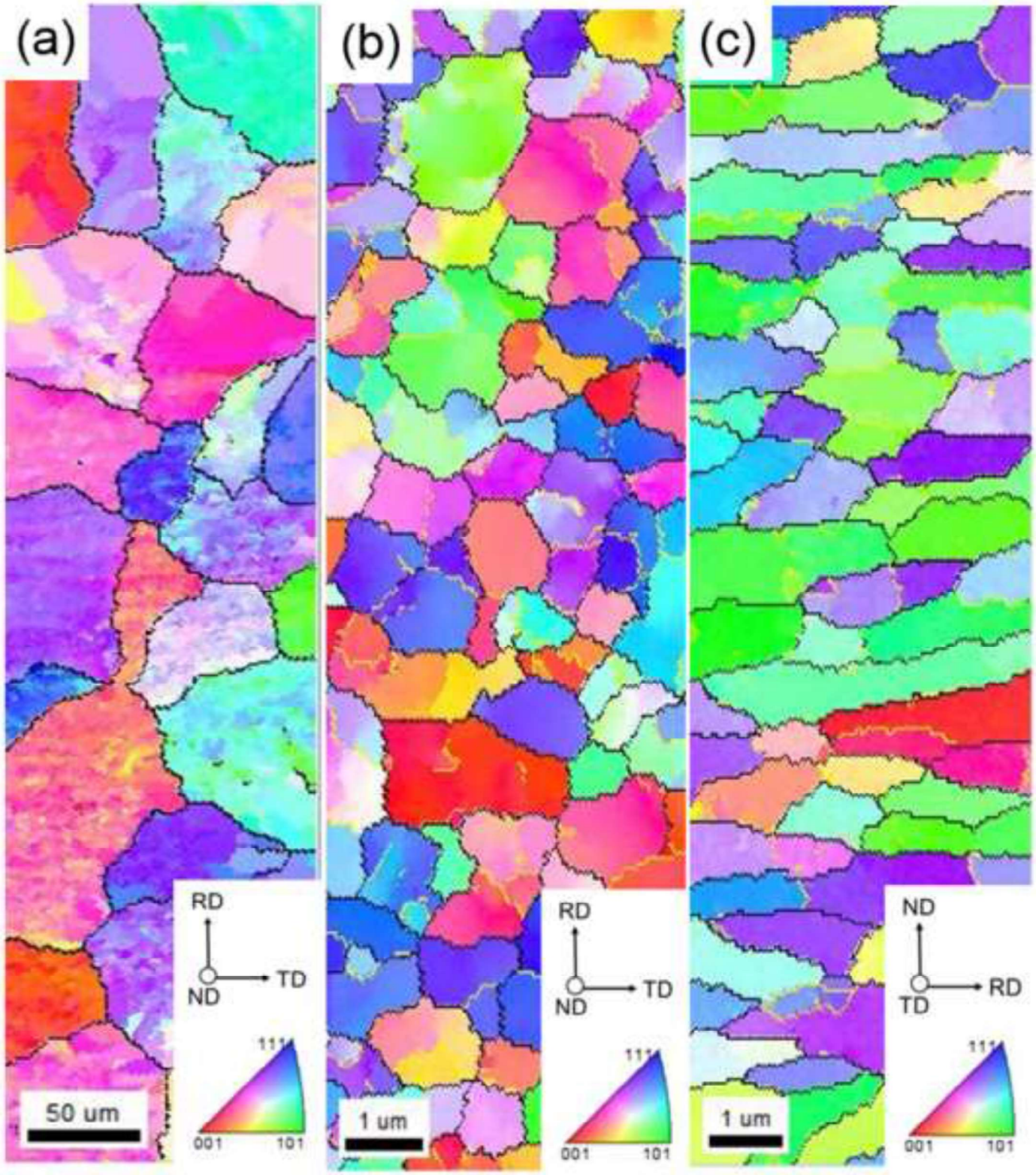

Figure
Click here to download high resolution image

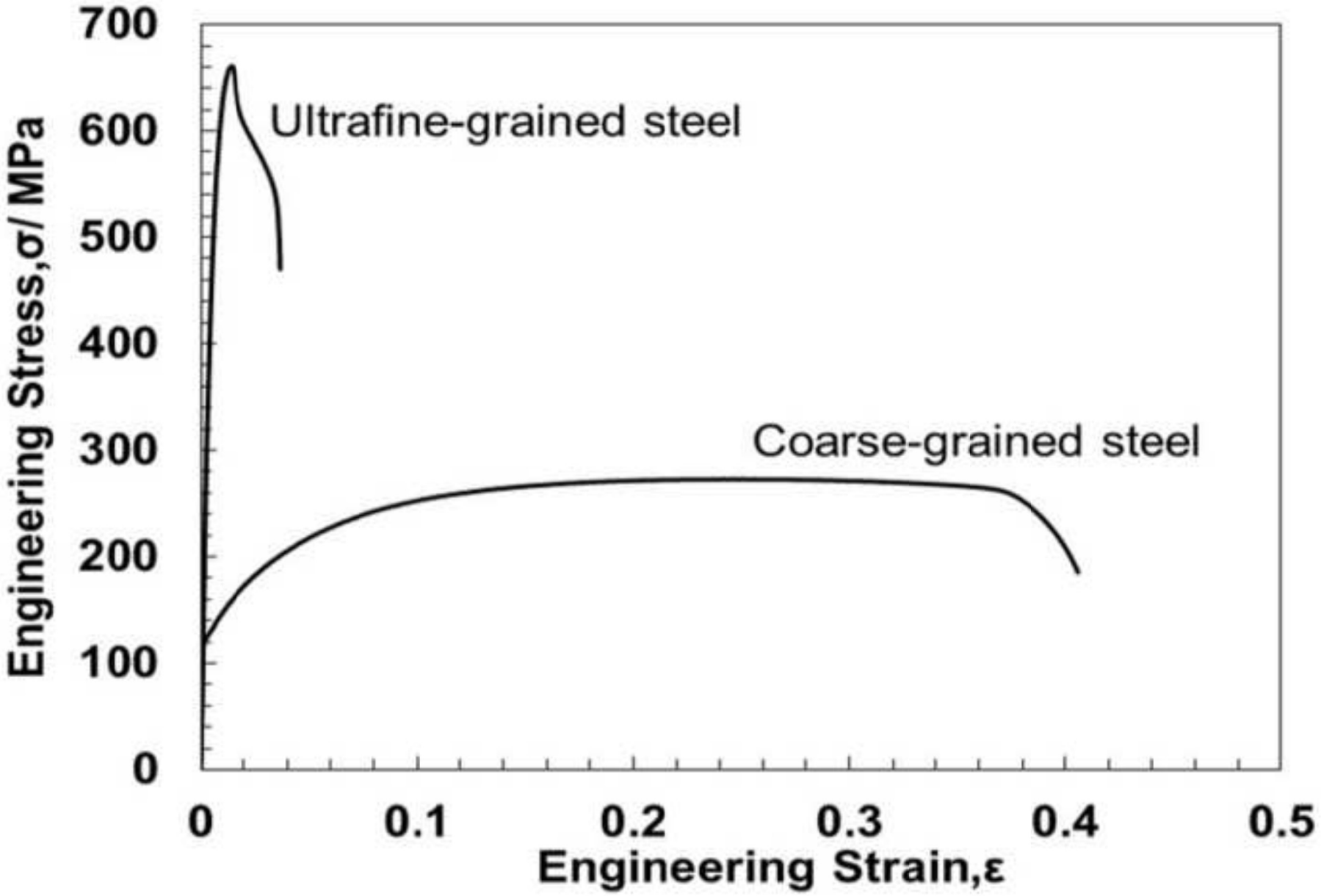

Figure
Click here to download high resolution image

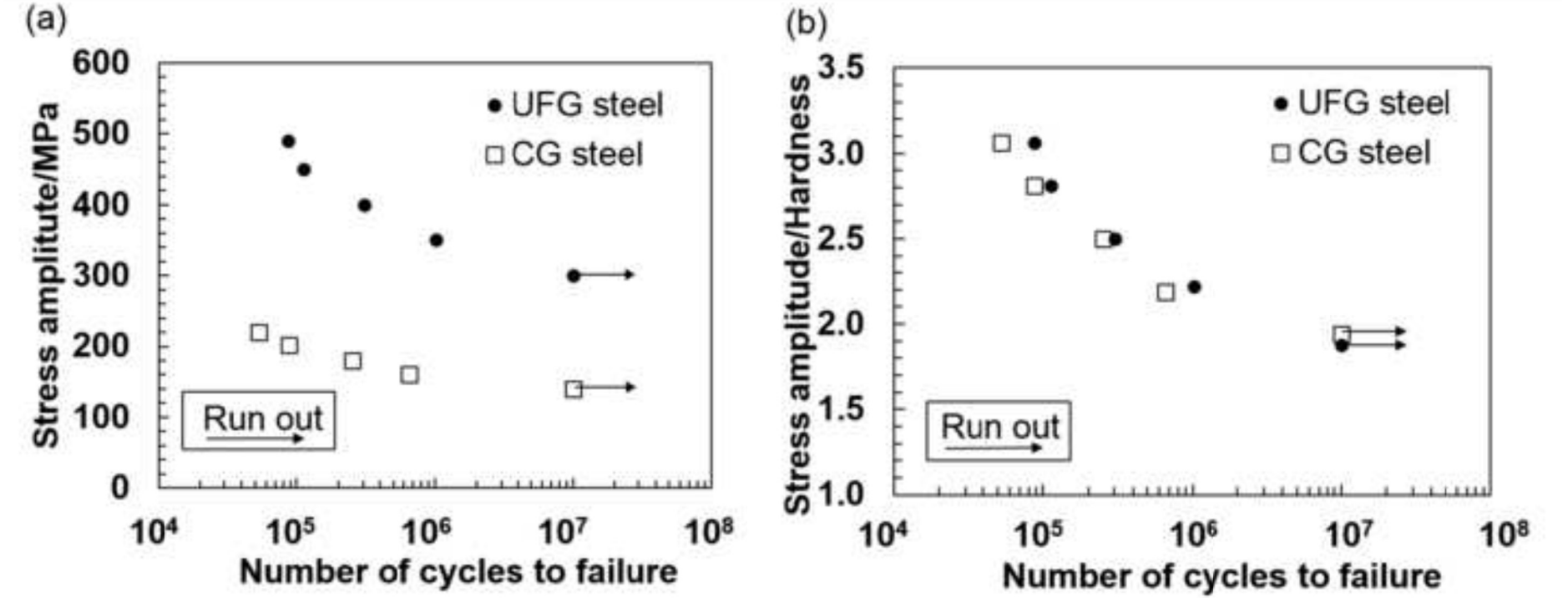

Figure
Click here to download high resolution image

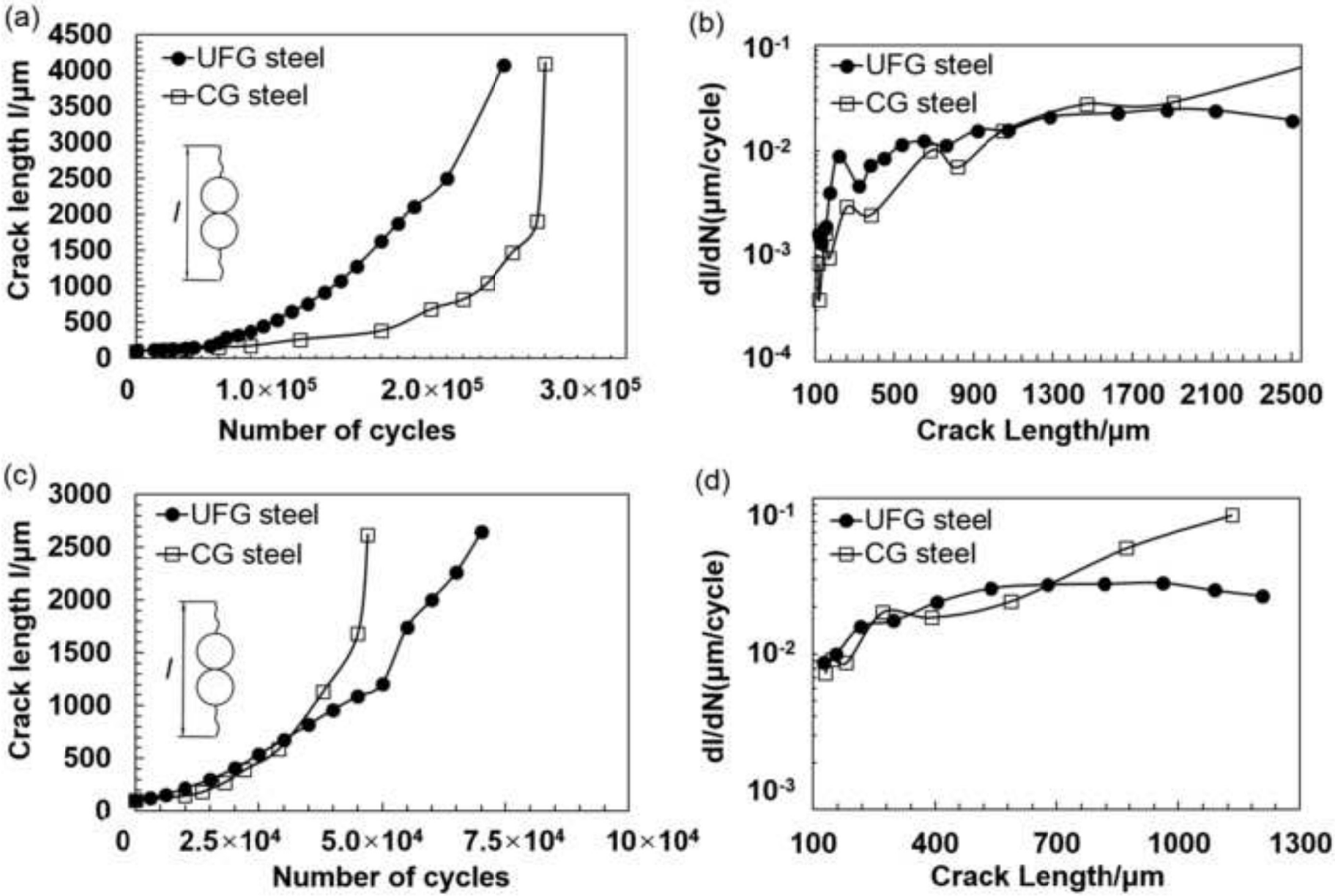

Figure
Click here to download high resolution image

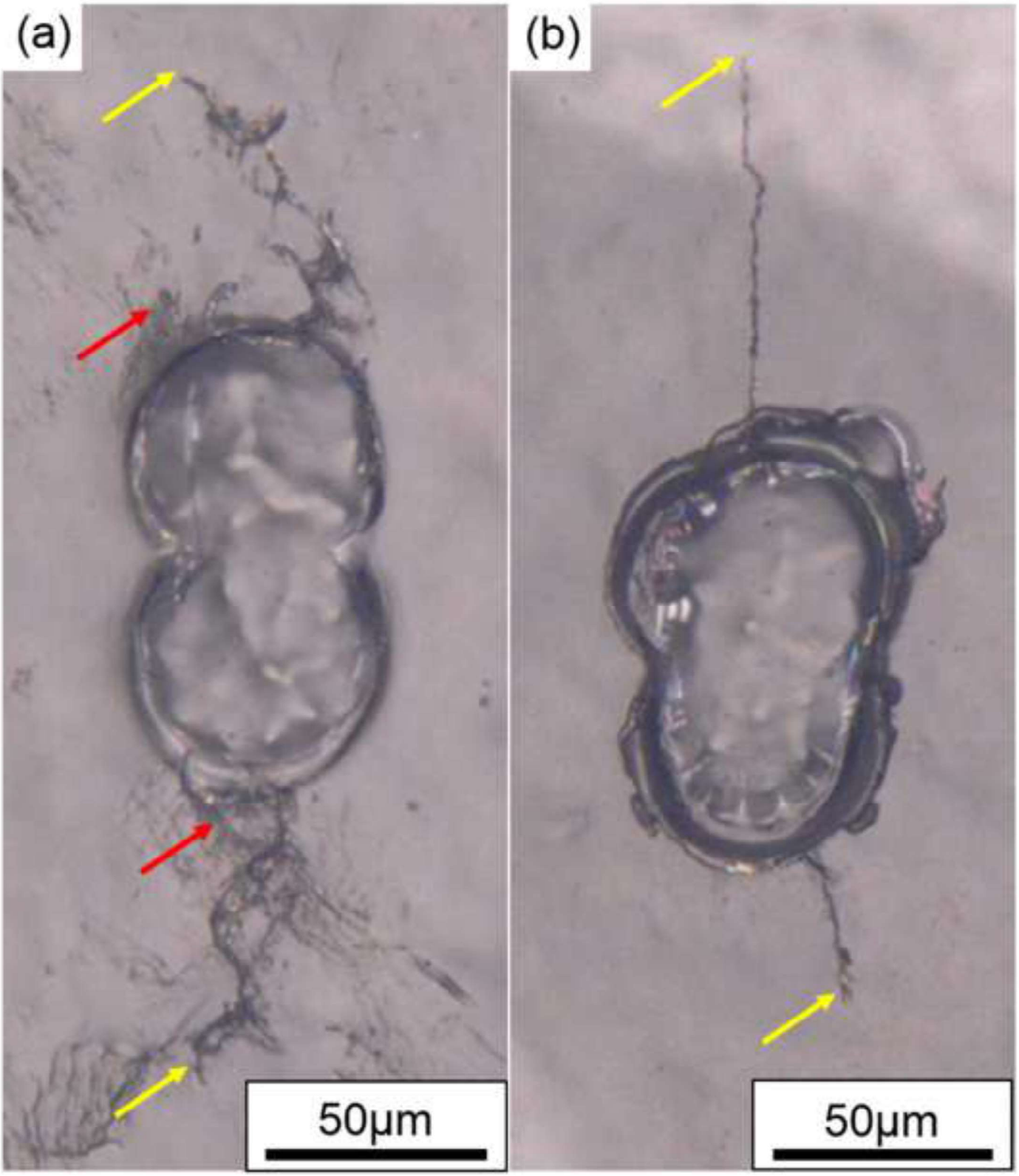

Figure
Click here to download high resolution image

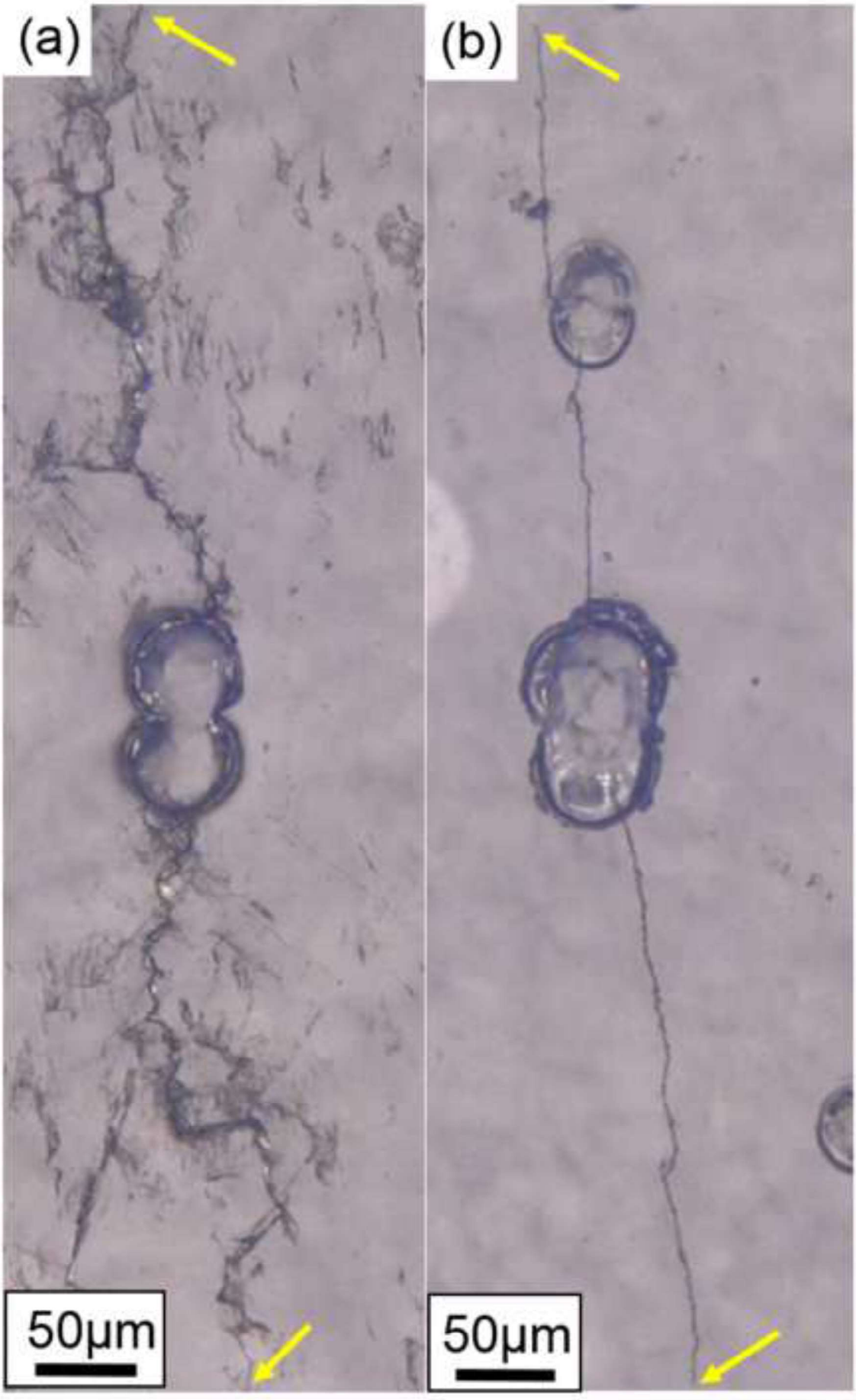

Figure
Click here to download high resolution image

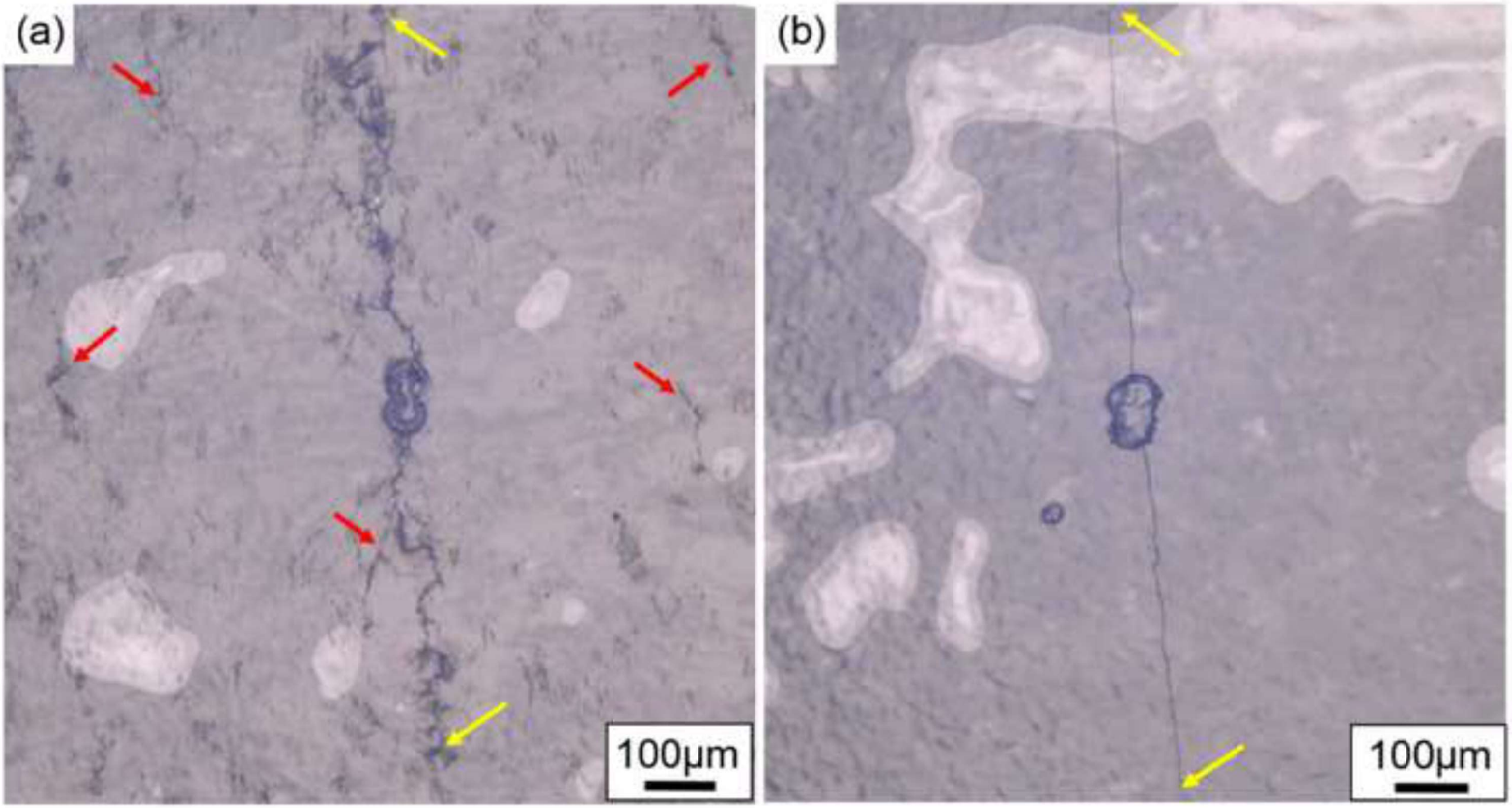

Figure
Click here to download high resolution image

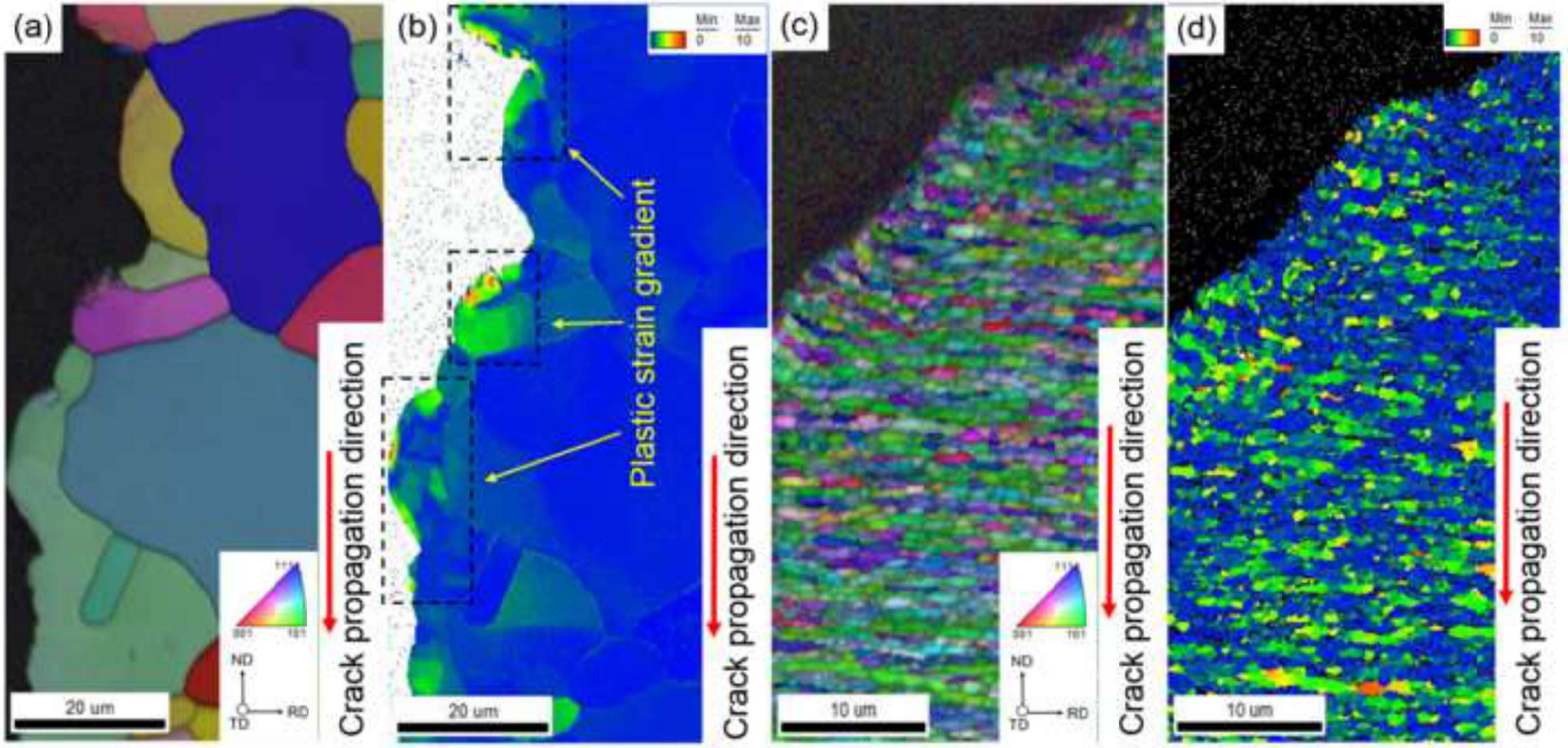

Figure
Click here to download high resolution image

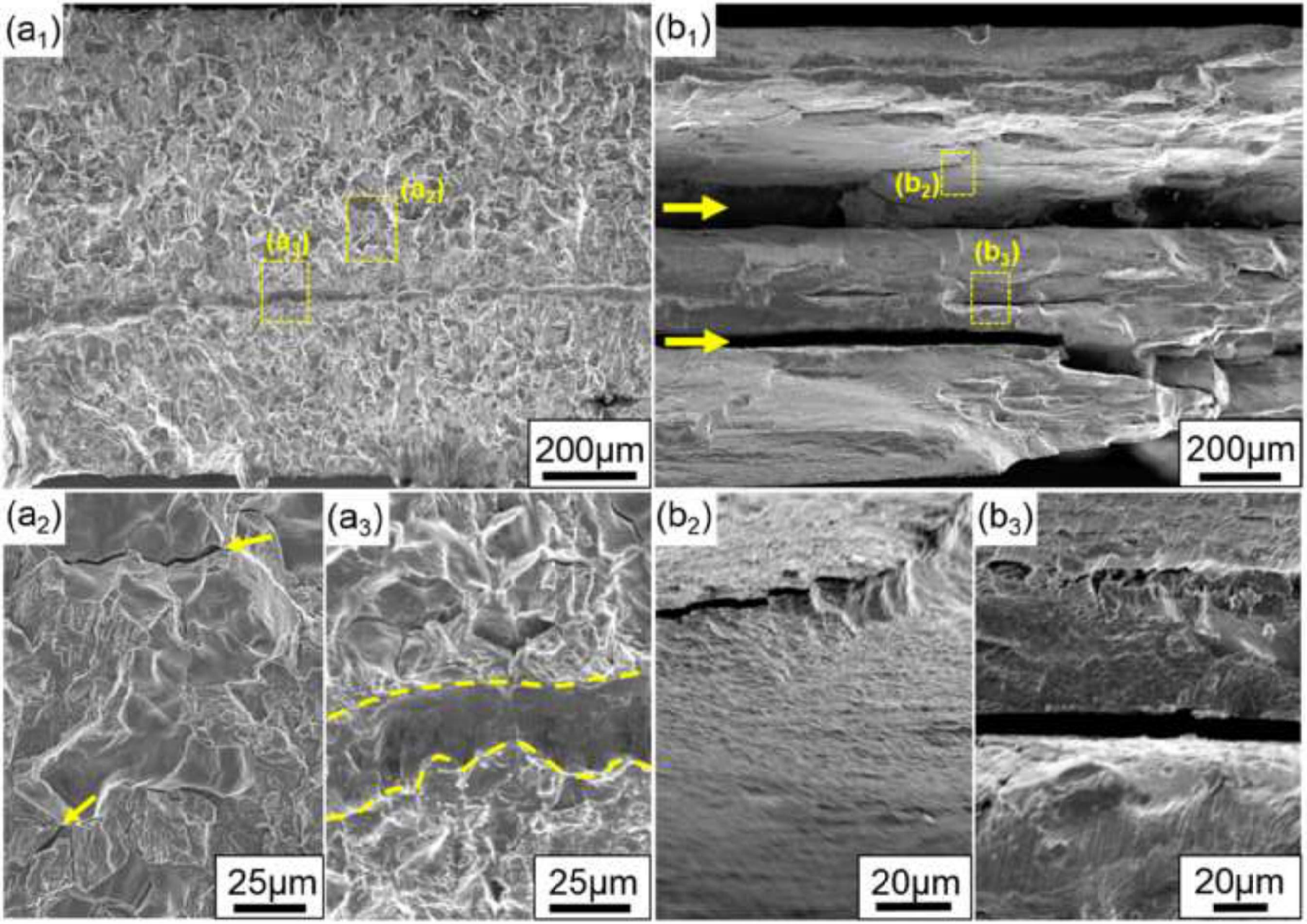

Figure
Click here to download high resolution image